Available online at www.sciencedirect.com
ScienceDirect
Journal of Solid State Chemistry 180 (2007) 2067–2074
JOURNAL OF SOLID STATE CHEMISTRY
www.elsevier.com/locate/jssc

Synthesis, characterization, photoluminescence and EPR investigations of Mn doped $MgAl_2O_4$ phosphors

Vijay Singh[a,*], R.P.S. Chakradhar[b], J.L. Rao[c], Dong-Kuk Kim[a,*]

[a]*Department of Chemistry, Kyungpook National University, Daegu 702701, Republic of Korea*
[b]*Glass Technology Lab, Central Glass and Ceramic Research Institute, Kolkata 700032, India*
[c]*Department of Physics, Sri Venkateswara University, Tirupati 517502, India*

Received 13 March 2007; received in revised form 26 April 2007; accepted 30 April 2007
Available online 21 May 2007

Abstract

$MgAl_2O_4$:Mn phosphors have been prepared at 500 °C by combustion route. Powder X-ray diffraction (XRD) indicated the presence of mono-$MgAl_2O_4$ phase. Scanning electron microscopy showed that the powder particle crystallites are mostly angular. Fourier transform infrared spectroscopy confirmed the presence of AlO_6 group which makes up the $MgAl_2O_4$ spinel. Photoluminescence studies showed green/red emission indicating that two independent luminescence channels in this phosphor. The green emission at 518 nm is due to $^4T_1 \rightarrow {}^6A_1$ transition of Mn^{2+} ions. The emission at 650 nm is due to the charge-transfer deexcitation associated with the Mn ion. EPR spectrum exhibits allowed and forbidden hyperfine structure at $g = 2.003$. The $g \approx 2.00$ is due to Mn^{2+} ion in an environment close to tetrahedral symmetry. It is observed that N and χ increase with decrease of temperature obeying the Boltzmann law. The variation of zero-field splitting parameter (D) with temperature is evaluated and discussed.

Keywords: Luminescence; EPR; Doping; Phosphor; Manganese; Combustion

1. Introduction

Magnesium aluminate oxide ($MgAl_2O_4$) spinel has been widely studied as it has a specific combination of desirable properties such as: excellent optical properties, high melting point (2135 °C), high chemical inertness against both acidic and basic slags, good mechanical strength at room temperature as well as high temperatures, low thermal expansion, low dielectric constant and good catalytic properties [1–5]. Therefore, it has been extensively used for various purposes as refractory material, structural material in fusion reactors, steel ladles, luminescent host, cement rotary kilns, vacuum induction furnaces, catalyst or catalyst support in the field of environmental catalysis, active element in humidity sensors and excellent transparent ceramic material for high-temperature arc-enclosing envelops, etc. [6–10].

The $MgAl_2O_4$ spinel belongs to the cubic space group O_h^7 ($Fd3\,m$) with eight formula units per unit cell. The first octant contains an Mg^{2+} ion at the center and has a tetrahedral coordination of O^{2-} ions with full T_d symmetry (A-site); the second octant has a six-fold distorted octahedral coordination of Al^{3+} ion belonging to the D_{3d} point group (B-site). Recently, significant efforts have been devoted by several research groups focusing on persistent phosphorescence [11], optically stimulated luminescence [12,13], absorption and photoluminescence [14], irradiation effect by neutron [15], etc. Luminescence of $MgAl_2O_4$ host is possible by the addition of rare earth or transition elements. Details of electronic states of doped transition-metal ions are understood through their electron spin resonance (ESR) spectrum [16].

Due to its wide and varied applications, the synthesis and properties of $MgAl_2O_4$ have been the focus of recent research. In the traditional method for the synthesis of this spinel, powders were prepared by solid-state reaction process using MgO and Al_2O_3 as starting materials [17,18]. In the solid-state process, the mixture of MgO

*Corresponding authors.
E-mail addresses: vijayjiin2006@yahoo.com (V. Singh), kimdk@knu.ac.kr (D.-K. Kim).

0022-4596/$ - see front matter © 2007 Elsevier Inc. All rights reserved.
doi:10.1016/j.jssc.2007.04.030

and Al_2O_3 is usually calcined for several hours in the temperature range of 1400–1600 °C to ensure the formation of this phase. However, this method is expensive and time-consuming which necessitates exploration of alternate techniques which are economically viable. Most of these achievements have been made by using sol–gel processing [19] and chemical co-precipitation [20]. These processes can indeed successfully reduce the formation temperature and processing time. In the literature, there are only few reports describing the low-temperature synthesis of Mn-doped $MgAl_2O_4$.

As a part of our programme on aluminate oxides [21–23], here we report a simple, fast, low-temperature initiated and safe combustion process for manganese-doped $MgAl_2O_4$ phosphors. Mn-doped materials have been studied extensively as they give green and red fluorescence [24–26]. Mn dopant does not affect the thermal stability and phase compositions of the parent aluminates [27,28]. It was also found that Mn^{2+} ions act as efficient activator ions in several hosts, since they show a highly saturated color, high luminescence efficiency and can be excited by all common excitation methods such as UV-irradiation, X-ray and electric field [29–31]. The prepared undoped $MgAl_2O_4$ and Mn-doped $MgAl_2O_4$ powder phosphors have been characterized by X-ray diffraction (XRD), scanning electron microscopy (SEM) and Fourier transform infrared spectroscopy (FTIR) techniques. Photoluminescence (PL) and electron paramagnetic resonance (EPR) studies have also been performed on the prepared phosphors.

2. Experimental

5 g $Al(NO_3)_3.9H_2O$, 1.7075 g $Mg(NO_3)_2.6H_2O$ and 2.6624 g CH_4N_2O were used to prepare $MgAl_2O_4$. The doped material was prepared using 5 g $Al(NO_3)_3.9H_2O$, 1.6918 g $Mg(NO_3)_2.6H_2O$, 2.6624 g CH_4N_2O and 0.0131 g $MnCl_2.4H_2O$ and had a chemical formula $Mg_{0.99}Al_2O_4:Mn_{0.01}$. The starting materials were mixed in an agate mortar to form a paste which was then transferred to a China dish. The dish containing the paste was introduced into a muffle furnace. Within minutes the paste foamed and flame produced lasting for several seconds. Urea speeds up the combustion process. After the nitrates and urea were heated to 500 °C, the sample temperature reached more than 1000 °C within few seconds due to the combustion process enhanced by the urea. The entire combustion process was completed in less than 5 min. The China dish was immediately removed from the furnace. Resultant voluminous product was crushed into powder using pestle and mortar and the resulting fine powder was used for characterization.

Powder XRD pattern was recorded using a Philips X'pert X-ray diffractometer with graphite monochromatized CuK_α radiation ($\lambda = 0.15418$ nm) and nickel filter at a scanning step of 0.03°, in the 2θ range of 10–70°. The morphology of the powders was obtained using a Hitachi S-4300 scanning electron microscope (SEM). FTIR spectra were taken using a Perkin-Elmer Rx1 instrument in the range 4000–400 cm^{-1}. Room temperature photoluminescence (PL) of the prepared phosphors was studied using a Hitachi F-4500 FL Spectrophotometer. EPR measurements were carried out using a Bruker EMX 10/12 X-band ESR spectrometer.

3. Results and discussion

3.1. X-ray diffraction

The XRD pattern for $MgAl_2O_4$ and $MgAl_2O_4$:Mn is shown in Figs. 1a and b, respectively. All diffraction peaks could be indexed to the single phase of $MgAl_2O_4$ and matched perfectly with the standard pattern (JCPDS 77-0435; Fig. 1c). The peaks and intensities of the produced powder and that of standard were the same. This indicates that there is a complete formation of spinel phase in both the samples at the furnace temperature (500 °C), and a further calcination treatment is not necessary. The values of the lattice constant '*a*' of the $MgAl_2O_4$ and $MgAl_2O_4$:Mn spinel as calculated from XRD data were 8.081 Å and 8.083 Å, respectively. The calculated cell parameters are in good agreement with the literature value of $a = 8.080$ Å (JCPDS 77-0435). The introduction of Mn (1%) does not change the lattice constant of $MgAl_2O_4$. There is no detectable trace of impurity in both samples.

3.2. Scanning electron microscopy

The microstructure of the combustion powders is analyzed using SEM (Fig. 2). The morphology of the undoped (Figs. 2a–d) and doped (Figs. 2e–h) powders remains almost the same. The powder particle crystallites are mostly angular (Figs. 2a and e). Besides the angular

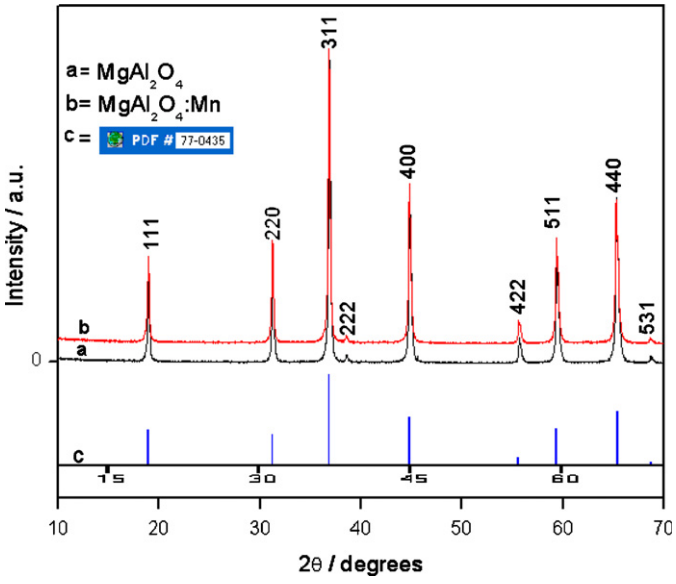

Fig. 1. Powder XRD patterns of (a) $MgAl_2O_4$ (b) $Mg_{0.99}Mn_{0.01}Al_2O_4$ and (c) reference $MgAl_2O_4$.

crystals, the powders also contained pores (Figs. 2b and f) because of the escaping gases during combustion reaction. This non-uniform particle size is caused due to the non-uniform distribution of temperature and mass flow during combustion. Magnified view of a pore of Fig. 2b (of undoped powder) is shown in Fig. 2c. The pore has a diameter close to 600 nm with several particles in the size range of 150–400 nm, nearby. The doped powder also contained pores of the diameter of 600 nm (Fig. 2g). The pores are formed due to the escape of the gases which are also formed as products of combustion. From the size measurements, it is clear that this method of synthesis can produce powder containing nanoparticles. There are some portions containing pores while the pores are also absent or very few in some areas (Figs. 2d and h).

3.3. FTIR

The FTIR spectra recorded for $MgAl_2O_4$ and $MgAl_2O_4$:Mn powders in the range 4000–400 cm^{-1} are shown in Fig. 3. Common bands exist for both the doped and undoped samples. The band around 3440 cm^{-1} corresponds to that of (O–H) vibration of H_2O. The band observed at 1629 cm^{-1} is attributed to the bending mode of H–O–H vibrations. There are sharp and distinct bands around 690 and 530 cm^{-1} indicating the presence of $MgAl_2O_4$ [32] and are in agreement with the XRD pattern (Fig. 1). These bands correspond to the AlO_6 groups, which build up the $MgAl_2O_4$ spinel.

Our FTIR spectra are similar to that of $MgAl_2O_4$ spinels produced by different preparation methods [32]. However, for a similar sample produced by polymerization method (involving a lengthy processing time), these peaks were not clear [33] and post-calcination at 700 °C produced these two peaks which were also not sharp. It is significant that our synthesis method involved a lower temperature of 500 °C, very short processing time and produced powder sample showing two sharp bands at 690 and 530 cm^{-1} indicating the formation of $MgAl_2O_4$ spinel. Post-calcination was not required in our case.

3.4. Photoluminescence studies

Room temperature photoluminescence spectra of undoped ($MgAl_2O_4$) and Mn-doped $MgAl_2O_4$ are shown in

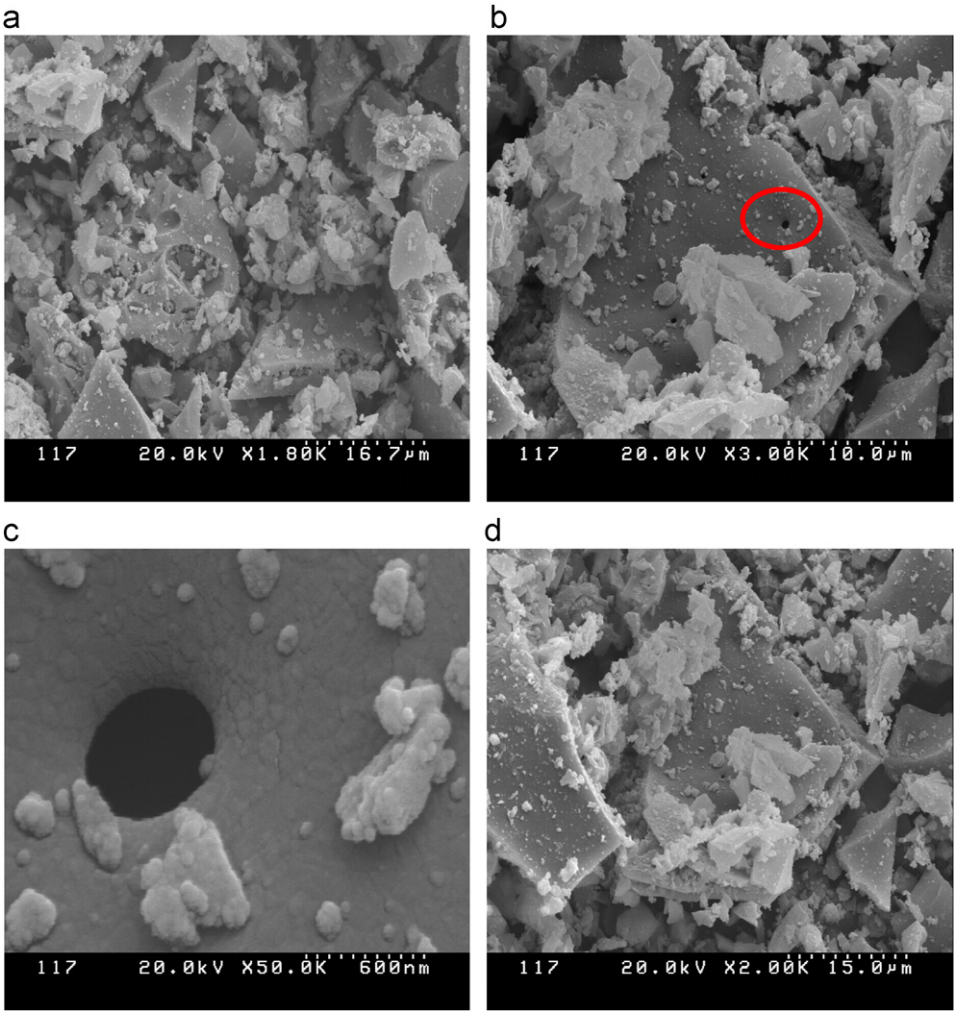

Fig. 2. SEM images of (a–d) $MgAl_2O_4$ and (e–h) $Mg_{0.99}Mn_{0.01}Al_2O_4$.

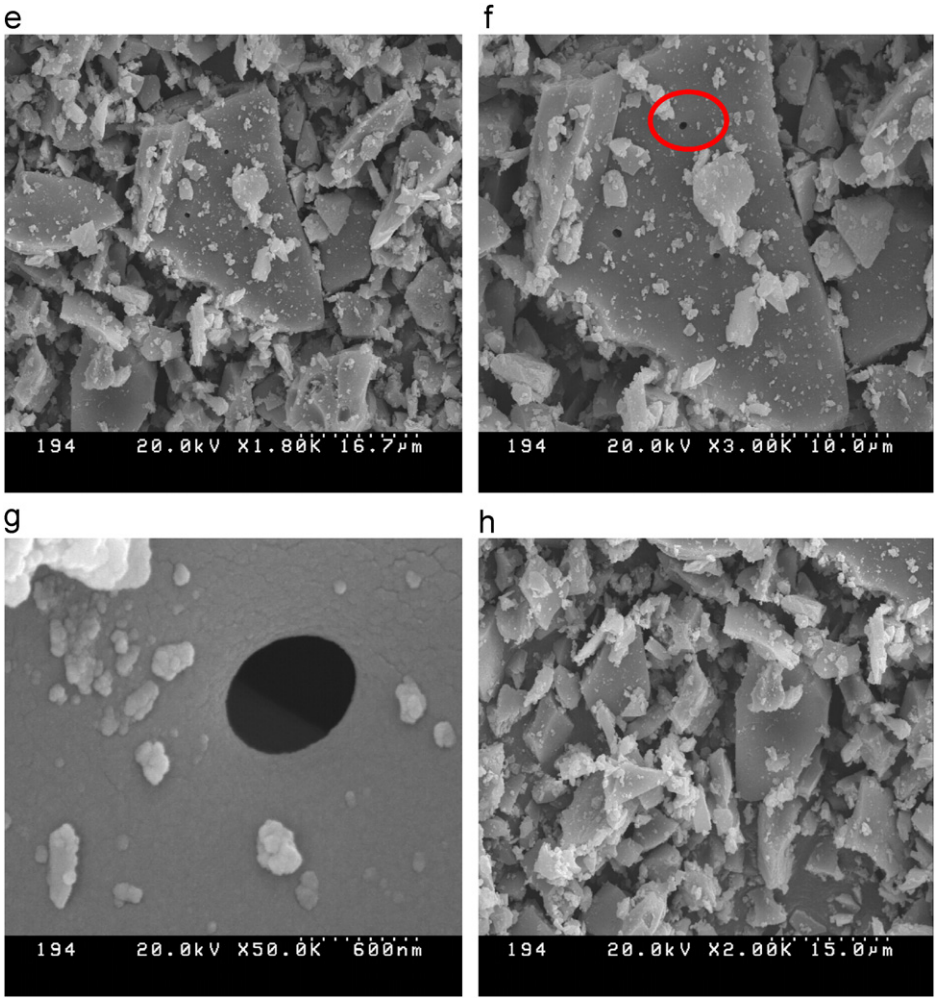

Fig. 2. (*Continued*)

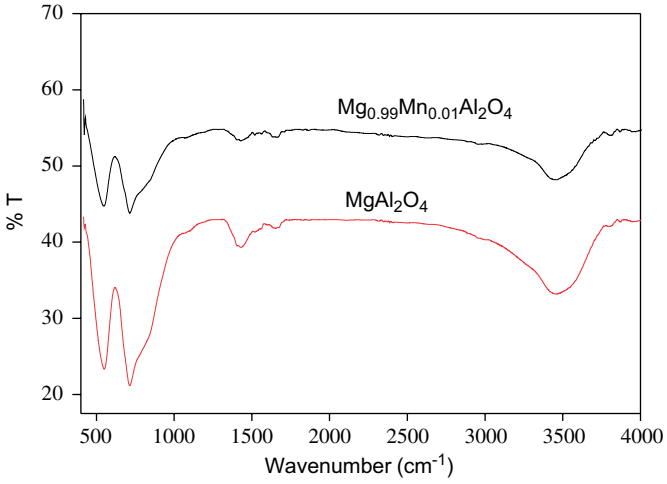

Fig. 3. FTIR spectra of $MgAl_2O_4$ and $Mg_{0.99}Mn_{0.01}Al_2O_4$.

Fig. 4. In the case of undoped $MgAl_2O_4$, the emission spectrum for excitation wavelength of 451 nm did not show any peak (Fig. 4, black line). However, the optical response of Mn-doped $MgAl_2O_4$ phosphor exhibits two interesting features, viz., (1) the *d–d* transition at 518 nm and optical processes involving the charge-transfer excitation around 650 nm are observed to coexist in the emission spectra; (2) the *d–d* transition is assigned to the spin-forbidden transitions among Mn^{2+} $(3d)^5$ configuration while the emission around 650 nm to the charge-transfer deexcitation associated with the Mn ion.

The emission processes at 518 and 650 nm can be seen to be independent from each other. In order to confirm, the authors also performed the PL experiments of excitation spectra for the emission at 650 nm as shown in Fig. 5. It is interesting to note that the excitation spectrum shows a peak at 313 nm. On the other hand, the emission at 650 nm in the longer wavelength region is observed under pumping at 313 nm. Therefore in Mn-doped $MgAl_2O_4$ phosphor, it is interesting to point out that the shorter wavelength emission (518 nm) is induced by the longer wavelength pumping (451 nm) while the longer wavelength emission (650 nm) is brought about by the shorter wavelength pumping (313 nm). These facts tell us that there are two independent emission channels in Mn-doped $MgAl_2O_4$ phosphor.

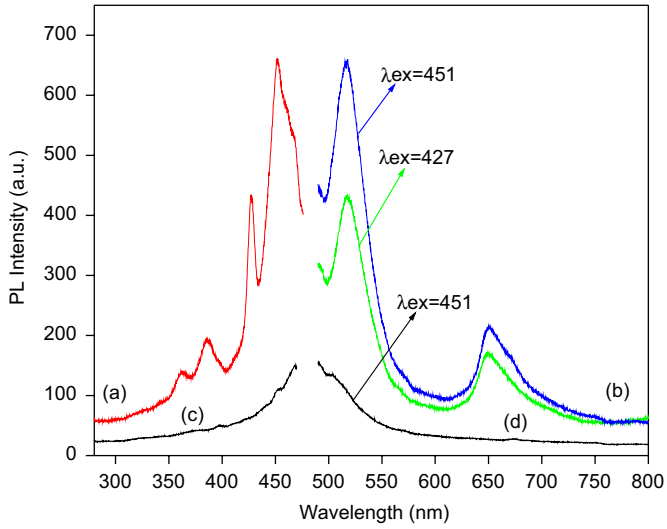

Fig. 4. Photoluminescence spectra of the doped and undoped $MgAl_2O_4$ ($\lambda_{em} = 518$ nm). (a) excitation spectra of $Mg_{0.99}Mn_{0.01}Al_2O_4$, (b) emission spectra of $Mg_{0.99}Mn_{0.01}Al_2O_4$, (c) excitation spectra of $MgAl_2O_4$, and (d) emission spectra of $MgAl_2O_4$.

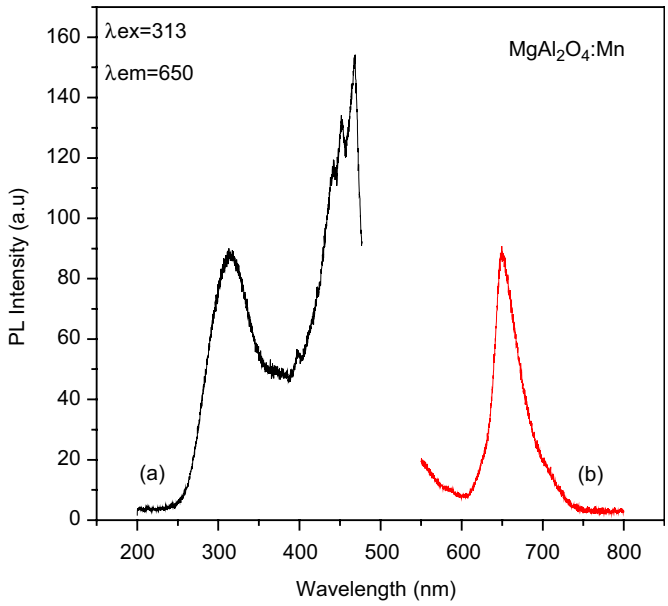

Fig. 5. Photoluminescence spectra of $Mg_{0.99}Mn_{0.01}Al_2O_4$, (a) excitation spectra, ($\lambda_{em} = 650$ nm), (b) emission spectra, ($\lambda_{ex} = 313$ nm).

The emission band peak at 518 nm is intense and is typical of Mn^{2+}, which is due to the $^4T_1$ (^4G) $\rightarrow$ $^6A_1$ (^6S) transition of Mn^{2+} ions. The emission around 650 nm is induced mainly by the band edge excitation around 313 nm and only weakly by the *d–d* transition around 451 nm. The excitation spectra corresponding to 518 nm emission, exhibit broad excitation peaks at 360, 386, 427 and 451 nm (Fig. 4(a)). These are due to the transitions from the multiplets ^4E (*D*), $^4T_2$ (*D*), $^4A_1$(*G*) ^4E(*G*) and $^4T_2$(*G*), respectively, to the ground state $^6A_1$ (^6S) of Mn^{2+} in tetrahedral coordination.

The emission process at 650 nm may be assigned to charge-transfer deexcitation associated with Mn^{2+} ion. The emission process can be explained as follows; the $MgAl_2O_4$ spinel may contain a finite density of Mg deficiencies. The Mg^{2+} deficiency is compensated by Mn^{2+} doping, so that the optical quality is improved by Mn-doping. This coincides with the assignment of Mn^{2+} ion to T_d (*A*) site. When the electron–hole pair is optically created, Mn^{2+} in *A* site attracts a hole at first so that Mn^{3+} state, i.e.,($3d^4$) is made as an intermediate state and an electron in the conduction band is radiatively annihilated resulting in the electronic ground state Mn^{2+} ($3d^5$). Conversely, there is a possibility for the electron in the conduction band to be trapped at Mn^{2+} ion at first as intermediate state and secondly the hole in the valence band is radiatively annihilated resulting in the electronic ground state Mn^{2+} state ($3d^5$). In both processes, the electron trapping or the hole trapping processes occur with the large probability amplitude because (a) the (3*d*)-orbital of Mn ion is well overlapped with O-2p_σ orbital which composes the valence band, and (b) the conduction band which is made of mainly Al^{3+} (3*s*) and (3*p*) and/or Mg^{2+} (3*s*) orbital is well hybridized with higher energy orbital of Mn^{2+} ion substituting Mg^{2+} ion.

$MgAl_2O_4$:Mn (1%) spinel has been reported to emit green emission peaking at about 511 nm, in the emission range of 480 to 650 nm [34]. Our studies showed peak position at 518 nm. Recently, Tomita et al. [16] have reported an emission peak at 520 and 650 nm for single crystals of $MgAl_2O_4$ doped with manganese grown by the floating zone method with heating source of Xe-lamp. Herein they have also reported two independent luminescence channels in Mn-doped $MgAl_2O_4$ crystal, similar to our studies.

3.5. Electron paramagnetic resonance studies

No EPR signal was detected in the spectra of undoped $MgAl_2O_4$ indicating that the starting materials used in the preparation are free from paramagnetic impurities. When manganese ions were introduced into the $MgAl_2O_4$ matrix the EPR spectra of all the investigated samples exhibit resonance signals due to Mn^{2+} ($3d^5$:$^6S_{5/2}$) ions entering the matrix as paramagnetic species. Fig. 6 shows the EPR spectrum of $MgAl_2O_4$:Mn phosphor at room temperature. The spectrum of Mn^{2+} ions in $MgAl_2O_4$ phosphor exhibits a broad resonance at $g \approx 2.003$, shows a six-line hyperfine structure (hfs), which is due to the interaction of electron spin of manganese ions with its own nuclear spin $I = 5/2$. The ability to observe the ^{55}Mn hyperfine structure has two tangible benefits: (1) it generally allows unambiguous assignments of positions of complex resonance lines to manganese and (2) the magnitude of the hyperfine splitting constant provides a measure of the bonding between Mn^{2+} ions and its surrounding ligands [35,36]. It is interesting to note that, EPR spectrum of Mn^{2+} ions in $MgAl_2O_4$ phosphor shows

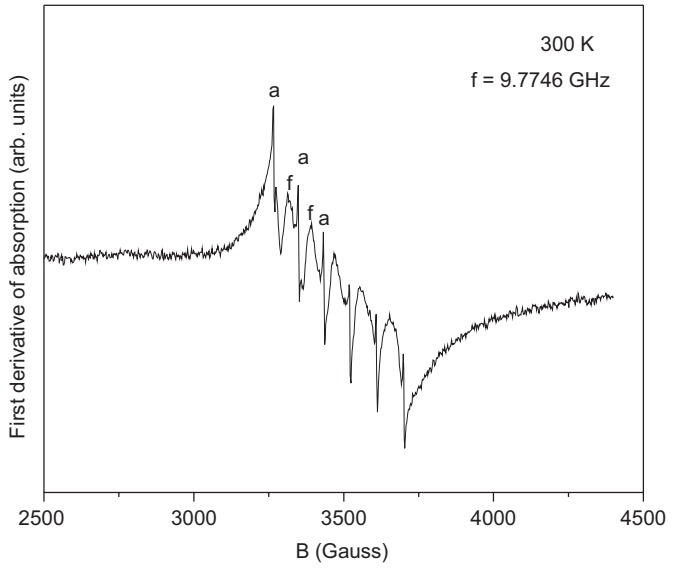

Fig. 6. EPR spectrum of $Mg_{0.99}Mn_{0.01}Al_2O_4$ phosphor at room temperature. The allowed and forbidden lines are denoted by 'a' and 'f', respectively.

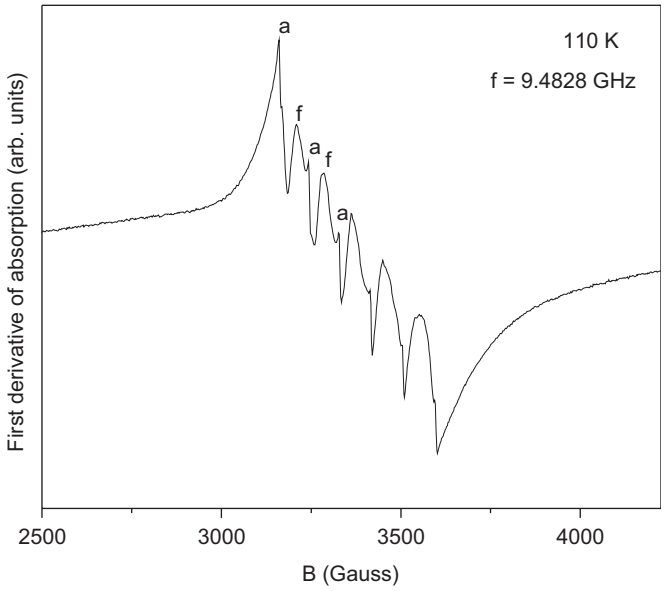

Fig. 7. EPR spectrum of $Mg_{0.99}Mn_{0.01}Al_2O_4$ phosphor at 110 K. The allowed and forbidden lines are denoted by 'a' and 'f', respectively.

forbidden lines in between the allowed hyperfine lines of the sextet (Fig. 6). Therefore the hyperfine spectrum of Mn^{2+} ions in $MgAl_2O_4$ phosphor will consist of six lines with respect to the selection rule $\Delta m_I = 0$ corresponding to the $\frac{1}{2} \leftrightarrow -\frac{1}{2}$ fine-structure transition. Besides this, there will be forbidden doublets corresponding to $\Delta m_I = \pm 1$. These forbidden hyperfine lines might come from level mixing arising from the second order perturbation which includes the cross product of the hyperfine coupling (A) and the axial zero field splitting parameter (D) [37]. In such cases, there must be some distortion that lowers symmetry from the cubic structure.

In case of d^5 transition metal ions, it is known that axial distortion of octahedral symmetry gives rise to three Kramers doublets $|\pm\frac{5}{2}>$, $|\pm\frac{3}{2}>$ and $|\pm\frac{1}{2}>$ [37]. Application of a Zeeman field lifts the spin degeneracy of the Kramer's doublets. As the crystal field splitting is normally much greater than the Zeeman field, the resonances observed are due to transitions within the Zeeman field split Kramers doublets. The resonance at $g \approx 2.0$ is due to the Mn^{2+} ions in an environment close to tetrahedral symmetry and is known to arise from the transition between the energy levels of the lower doublet.

Fig. 7 shows the EPR spectrum of $MgAl_2O_4$:Mn phosphor at 110 K. Further, it is observed that the intensity of the hyperfine lines increases with decreasing temperature in accordance with the Boltzmann law. Table 1 gives the spin-Hamiltonian parameter values for the Mn^{2+} ions in $MgAl_2O_4$ phosphor. The values of hyperfine splitting constant, A, were determined from the average value of hyperfine splitting of successively allowed hyperfine lines of the central sextet. It is apparent from different average values of A measured from peak-to-peak (A_{pp}) and trough-to-trough (A_{tt}), that the individual lines are strain broadened, leading to an asymmetry in the absorption spectrum [38]. The first derivative spectrum, as a consequence, shows larger values of A, when measured trough-to-trough, rather than peak-to-peak. An overall average was calculated from

$$A_{avg} = [(\Delta_{Opp} + \Delta_{Ott})/5 + (\Delta_{Mpp} + \Delta_{Mtt})/3 + (\Delta_{Ipp} + \Delta_{Itt})]/6, \quad (1)$$

where Δ_{Opp} and Δ_{Ott} represent the differences between the first and sixth peak positions, measured peak-to-peak and trough-to-trough, respectively. Δ_{Mpp} and Δ_{Mtt} represent difference in positions between second and fifth peaks and Δ_{Ipp} and Δ_{Itt} between second and third peaks. It is interesting to note that, in all of the samples, $\Delta_{Opp}/5 \approx \Delta_{Mpp}/3 \approx \Delta_{Ipp}$ and $\Delta_{Ott}/5 \approx \Delta_{Mtt}/3 \approx \Delta_{Itt}$.

The strength of the hyperfine splitting (A) depends on the matrix into which the ion is dissolved and is mainly determined by the electronegativity of the neighbors. This means a qualitative measure of the covalency of the bonding in the matrix which can be determined from the value of A; the smaller the splitting, the more covalent the bonding of the anion. From the measured A values it is apparent that the Mn^{2+} ion phosphor (with $A \approx 82$ G) is in moderately ionic environment.

3.6. Calculation of number of spins (N) participating in resonance

The number of spins participating in resonance can be calculated by comparing the area under the absorption curve with that of a standard ($CuSO_4.5H_2O$ in this study) of known concentration. Weil et al. [39] gave the following

Table 1
The spin-Hamiltonian parameters, number of spins participating in resonance (N), paramagnetic susceptibility (χ) and zero-field splitting parameter (D) for $Mg_{0.99}Mn_{0.01}Al_2O_4$ at room temperature and 110 K

System	Temperature (K)	g ($\pm$0.001)	A_{avg} (gauss)	$N \times 10^{21}$ (arb. units)	$\chi \times 10^{-4}$ ($m^3 Kg^{-1}$)	D (gauss)
$Mg_{0.99}Mn_{0.01}Al_2O_4$	300	2.003	81	0.303	0.74	308
$Mg_{0.99}Mn_{0.01}Al_2O_4$	110	2.003	83	1.538	3.76	323

expression which includes the experimental parameters of both sample and standard:

$$N = \frac{A_x(Scan_x)^2 G_{std}(B_m)_{std}(g_{std})^2[S(S+1)]_{std}(P_{std})^{1/2}}{A_{std}(Scan_{std})^2 G_x(B_m)_x(g_x)^2[S(S+1)]_x(P_x)^{1/2}}[Std], \quad (2)$$

where A is the area under the absorption curve, which can be obtained by double integrating the first derivative EPR absorption curve, *Scan* is the magnetic field corresponding to a unit length of the chart, G is the gain, B_m is the modulation field width, g is the g factor, S is the spin of the system in its ground state. P is the power of the microwave source. The subscripts 'x' and '*std*' represent the corresponding quantities for the Mn^{2+}:$MgAl_2O_4$ phosphor and the reference (($CuSO_4.5H_2O$) respectively. [Std] is the number of $CuSO_4.5H_2O$ molecules in the reference taken. The value of N has been calculated for the studied phosphor at room temperature and also at 110 K and are presented in Table 1. It is observed that when the temperature is decreased from RT to 110 K, the number of spins participating in resonance increases. This is due to variation of spin population with temperature, in accordance with the Boltzmann law.

3.7. Calculation of paramagnetic susceptibility (χ) from EPR data

The EPR data can be used to calculate the paramagnetic susceptibility of the sample using the formula [40]

$$\chi = \frac{Ng^2\beta^2 J(J+1)}{3k_B T}, \quad (3)$$

where N is the number of spins per m^3 and the other symbols have their usual meaning. N can be calculated from Eq. (2) and g is taken from EPR data. The paramagnetic susceptibility (χ) evaluated from EPR data are also presented in Table 1. The paramagnetic susceptibility was calculated using Eq. (3), one can observe that, the ratio between the susceptibility at 110 K and the susceptibility at 300 K should be equal to the ratio between $N(1\,1\,0)$ and $N(3\,0\,0)$. From the present study, the ratio of $N(1\,1\,0)/N(3\,0\,0)$ is 5 and thereby the ratio of susceptibilities is also 5 which is in good agreement with N. We chose to determine the spin susceptibility from EPR, because this technique has several advantages over a static measurement, where a diamagnetic contribution must be subtracted off.

3.8. Calculation of the zero-field splitting parameter (D) from EPR spectra

The intensity of hyperfine lines can be used to calculate the zero-field splitting parameter (D) from the ratio of allowed hyperfine lines (corresponding to the selection rule $\Delta m_I = 0$) using the formula [41].

$$I_m \propto 2\frac{A^2(35-4m^2)}{2(g\beta H)^2} - \frac{5.334D^2}{(g\beta H)^2} - \frac{35.14D^2(35-4m^2)}{(g\beta H)^2} + \frac{208D^4(35-4m^2)^2}{(g\beta H)^4}, \quad (4)$$

where m is the nuclear spin magnetic quantum number, I_m is the intensity of the mth allowed hyperfine (HF) line, A is the HF splitting constant, D is the zero-field splitting parameter and the rest of the symbols have their usual meaning.

The authors have calculated D values for $Mg_{0.99}Mn_{0.01}Al_2O_4$ phosphor at room temperature as well as at 110 K. The ratio of $\frac{5}{2} \leftrightarrow \frac{5}{2}$ hyperfine line intensity to that of the $\frac{3}{2} \leftrightarrow \frac{3}{2}$ hyperfine line is found to vary with temperature. The D values calculated from those ratios as a function of temperature are shown in Table 1. The D values obtained from the ratio of the allowed hyperfine line intensities ($\approx$300 G) is of the same order for as the D values of Mn^{2+} ions in different crystalline hosts [42–45].

The temperature dependence of D was discussed by several authors [42–45] for Mn^{2+} ions in crystalline environments. On the basis of the stress dependence of EPR spectra, Groen et al. [44] concluded that the potential well of Mn^{2+} ions is highly anharmonic. Hence vibrations of Mn^{2+} ions in these anharmonic potential wells (which results in thermal expansion) will be responsible for the variation of zero-field splitting parameters. Jain and Srinivasan [42] and Naramishulu and Rao [45] also concluded that the thermal contraction is the sole phenomenon that is responsible for the variation of D with temperature. In the present study, it is observed that the zero-field splitting parameter (D) is found to be sensitive to temperature. The observed increase in the zero-field splitting parameter (D) with decrease of temperature is probably due to distortion of ligands and the distortion increases with the decrease in temperature on account of lattice contraction [46].

4. Conclusions

The combustion method is found to be suitable for the synthesis of Mn-doped $MgAl_2O_4$ spinel. Combustion product could be prepared within several minutes at low temperature. This might be useful in lowering the cost of the material. The present results suggest that Mn doped $MgAl_2O_4$ phosphor has the potential to be used as green/red emitting phosphors. Several small particles having diameters of the order of 150–400 nm were observed. AlO_6 groups which are precursor to magnesium aluminate spinel were indicated by FTIR in the powder synthesized at 500 °C. It is interesting to observe from PL studies, the shorter wavelength emission (518 nm) is induced by the longer wavelength pumping (451 nm) while the longer wavelength emission (650 nm) is brought about by the shorter wavelength pumping (313 nm). These facts tell us that there are two independent emission channels in Mn-doped $MgAl_2O_4$ phosphor. The 650 nm emission is also partially induced by the *d–d* transition at 451 nm of Mn^{2+} ions. The EPR spectra of $MgAl_2O_4$:Mn phosphor exhibit an allowed as well as forbidden hyperfine structure at $g \approx 2.00$. The resonance signal at $g \approx 2.00$ is due to Mn^{2+} ion in an environment close to tetrahedral symmetry. The magnitude of hyperfine splitting constant (A) for Mn^{2+} ion indicates that the Mn^{2+} ion is in a moderately ionic environment. The observed increase in the zero-field splitting parameter (D) with decrease of temperature has been attributed to the shrinkage of the lattice at low temperatures.

Acknowledgments

This work was supported by Korea Research Foundation Grant KRF-2003-070-C00029. One of the authors (Vijay Singh) is thankful to the Kyungpook National University for their postdoctoral fellowship. Another author (RPSC) thanks Dr. H. S. Maiti, Director, CGCRI and Dr. K. K. Phani, Head, GTL lab, CGCRI for their encouragement.

References

[1] I. Ganesh, S. Bhattacharjee, B.P. Saha, R. Johnson, Y.R. Mahajan, Ceram. Int. 21 (2001) 773.
[2] J. Mori, W. Watanabe, M. Yoshimura, Y. Oguchi, T. Kawakami, Bull. Am. Ceram. Soc. 69 (7) (1990) 1172.
[3] I. Ganesh, S. Bhattacharjee, B.P. Saha, R. Johnson, R. Rajeshwari, M.V. Senguptta, R. Ramana, Y.R. Mahajan, Ceram. Int. 28 (2002) 245.
[4] C. Baudin, R. Martinez, P. Pena, J. Am. Ceram. Soc. 78 (7) (1995) 1857.
[5] Y.C. Kang, J.S. Chio, S.B. Park, J. Eur. Ceram. Soc. 18 (1998) 61.
[6] N. Seiyama, N. Yamazoe, H. Arai, Sens. Actuators 4 (1983) 85.
[7] H. Zhang, X. Jia, Z. Liu, Z. Li, Mater. Lett. 58 (2004) 1625.
[8] J. Sehested, A. Carlsson, T.V.W. Janssens, P.L. Hansen, A.K. Datye, J. Catal. 197 (2001) 200.
[9] E.H. Walker Jr., J.W. Owens, M. Etienne, D. Walker, Mater. Res. Bull. 37 (2002) 1041.
[10] J.A. Ball, M. Pirzada, R.W. Grims, M.O. Zaceta, D.W. Price, B.P. Uberuaga, J. Phys. Condens. Matt 17 (2005) 7621.
[11] D. Jia, W.M. Yen, J. Lumin. 101 (2003) 115.
[12] E.M. Yoshimura, E.G. Yukihara, Radiat. Meas. 41 (2006) 163.
[13] E.M. Yoshimura, E.G. Yukihara, Nucl. Instrum. Methods 250 (2006) 337.
[14] X.L. Duan, D.R. Yuan, X.F. Cheng, Z.M. Wang, Z.H. Sun, C.N. Luan, D. Xu, M.K. Lv, Opt. Mater. 25 (2004) 65.
[15] A. Ibarra, D. Bravo, M.A. Garcia, J. Llopis, F.J. Lopez, F.A. Garner, J. Nucl. Mater. 258–263 (1998) 1902.
[16] A. Tomita, T. Sato, K. Tanaka, Y. Kawabe, M. Shirai, K. Tanaka, E. Hanamura, J. Lumin. 109 (2004) 19.
[17] T. Bhatia, K. Chattopadhyay, V. Jayaram, J. Am. Ceram. Soc. 84 (8) (2001) 1873.
[18] R.J. Bratton, J. Am. Ceram. Soc. 52 (8) (1971) 141.
[19] O. Varnier, N. Hovnanian, A. Larbot, P. Bergez, L. Cot, J. Charpin, Mater. Res. Bull. 29 (1994) 479.
[20] G. Gusmano, P. Nunziante, E. Traversa, G. Chiozzini, J. Eur. Ceram. Soc. 7 (1991) 31.
[21] V. Singh, T.K. Gundu Rao, J.-J. Zhu, J. Lumin. 126 (2007) 1.
[22] V. Singh, T.K. Gundu Rao, J.-J. Zhu, J Solid State Chem 179 (2006) 2574.
[23] V. Singh, V. Natarajan, J.-J. Zhu, Opt. Mater. 29 (2007) 1447.
[24] A. Bergenstein, W.B. White, J. Electrochem Soc. 118 (1971) 1166.
[25] R. Morimo, R. Mochinaga, K. Nakamura, Mater. Res. Bull. 29 (1994) 751.
[26] T. Murata, T. Tanoue, M. Iwasaki, K. Morinaga, T. Hase, J. Lumin. 114 (2005) 207.
[27] M. Machida, K. Eguchi, H. Atai, Chem. Lett. 5 (1987) 767.
[28] G. Groppi, C. Cristiani, P. Forzatti, Catalysis 13 (1997) 85.
[29] T. Minami, T. Maeno, Y. Kuroi, S. Takata, Jpn. J. Appl. Phys. 34 (1995) L684.
[30] L.E. Shea, R.L. Datta, J.J. Brown, J. Electrochem. Soc. 141 (1994) 1950.
[31] B.A. Smith, J.Z. Zhang, Phys. Rev. B 62 (2000) 2021.
[32] J. Guo, H. Lou, H. Zhao, X. Wang, X. Zheng, Mater. Lett. 58 (2004) 1920.
[33] P.Y. Lee, H. Suematsu, T. Yano, K. Yatsui, J. Nanopart. Res. 8 (2006) 911.
[34] R. Clausen, K. Petermann, IEEE Quantum Electron. 24 (6) (1988) 1114.
[35] J.S. Van Wieringen, Discuss Faraday Soc. 19 (1955) 118.
[36] F.D. Tsay, L. Helmholz, J. Chem. Phys. 50 (1969) 2642.
[37] A. Abragam, B. Bleaney, Electron Paramagnetic Resonance of Transition Ions, Clarendon, Oxford, 1970.
[38] J.R. Pilbrow, Bull. Magn. Reson. 9 (1987) 32.
[39] J.A. Weil, J.R. Bolton, J.E. Wertz, Electron Paramagnetic Resonance—Elementary Theory and Practical Applications, Wiley, New York, 1994, p.498.
[40] N.W. Aschcroft, N.D. Mermin, Solid State Physics, Harcourt College Publishers, New York, 2001, p.656.
[41] B.T. Allen, J. Chem. Phys. 43 (1965) 3820.
[42] V.K. Jain, T.M. Srinivasan, Acta Phys. Pol. A 53 (1978) 779.
[43] R. Dayal, D. Ramachandra Rao, P. Venkateswarlu, Can. J. Phys. 56 (1978) 1175.
[44] J. Groen, G. van Opbroek, K. Post, H.W. den Hartog, Phys. Rev. B 30 (1984) 3608.
[45] K.V. Narasimhulu, J. Lakshmana Rao, Physica B 254 (1998) 37.
[46] W.M. Walsh Jr, J. Jeener, N. Bloembergen, Phys. Rev. (A) 139 (1965) 1338.